LETTERS
PUBLISHED ONLINE: 5 DECEMBER 2010 | DOI: 10.1038/NNANO.2010.235
nature nanotechnology

Freestanding palladium nanosheets with plasmonic and catalytic properties

Xiaoqing Huang[1], Shaoheng Tang[1], Xiaoliang Mu[1], Yan Dai[1], Guangxu Chen[1], Zhiyou Zhou[1], Fangxiong Ruan[2], Zhilin Yang[2] and Nanfeng Zheng[1]*

Ultrathin metal films can exhibit quantum size and surface effects that give rise to unique physical and chemical properties[1–7]. Metal films containing just a few layers of atoms can be fabricated on substrates using deposition techniques[7], but the production of freestanding ultrathin structures remains a significant challenge. Here we report the facile synthesis of freestanding hexagonal palladium nanosheets that are less than 10 atomic layers thick, using carbon monoxide as a surface confining agent. The as-prepared nanosheets are blue in colour and exhibit a well-defined but tunable surface plasmon resonance peak in the near-infrared region. The combination of photothermal stability and biocompatibility makes palladium nanosheets promising candidates for photothermal therapy. The nanosheets also exhibit electrocatalytic activity for the oxidation of formic acid that is 2.5 times greater than that of commercial palladium black catalyst.

Surface plasmon resonance (SPR) is an important property of metal nanostructures, and has been used in applications such as optical sensing of biomolecules and small molecules[8,9], photothermal therapy[10–12], spectral signal enhancement[13], photovoltaic conversion efficiency enhancement[14], optical waveguiding[15] and probing of catalytic reactions[16]. The SPR features of metal nanoparticles are highly sensitive to composition, size and morphology. For gold and silver, the synthesis of nanostructures with controlled size and morphology has led to the production of nanostructures with well-defined SPR absorption features that can be systematically tuned from the visible to the near-infrared (NIR) spectral range. The NIR SPR properties of metal nanostructures make them useful agents for cancer photothermal therapy using NIR lasers[10,11]. Nanorods, nanoshells, nanoprisms, nanoplates and nanocages/nanoboxes are the most common metal nanostructures to exhibit NIR SPR features[10,17–20]. Sophisticated synthetic techniques to prepare such anisotropic nanostructures have been used mainly for silver and gold. However, studies have shown that many anisotropic silver/gold nanostructures exhibiting NIR SPR lack good photothermal stability upon irradiation with high-power NIR lasers. The heat generated by NIR irradiation can melt the anisotropic silver/gold nanostructures into solid particles[21,22], leading to the loss of their NIR SPR. The chemical synthesis of alternative metal nanostructures with well-defined SPR peaks in the NIR is thus desirable, but remains a significant challenge[9].

In principle, palladium, because of its significantly higher bulk melting point ($MP_{Pd} = 1{,}828$ K versus $MP_{Ag} = 1{,}235$ K and $MP_{Au} = 1{,}337$ K), should show enhanced photothermal stability. Despite recent progress in the chemical synthesis of palladium nanostructures with various sizes and morphologies[23], currently available palladium nanostructures display no tunable SPR properties as have been widely discovered in gold and silver nanostructures. The palladium nanostructures chemically synthesized to date exhibit SPR only in the UV and visible regions; for example, Xia and colleagues have prepared palladium nanocages and nanoplates displaying broad SPR peaks in the visible region[24]. The absence of strong NIR SPR absorption has unfortunately precluded the use of palladium nanostructures in photothermal therapy using NIR lasers.

In this Letter, we report a general CO-confined growth method to prepare 'colloidal palladium blue', a freestanding form of ultrathin hexagonal palladium nanosheets displaying well-defined but tunable (826–1,068 nm) and strong SPR absorption (extinction coefficient, 4.1×10^9 M^{-1} cm^{-1}) in the NIR region. Owing to the growth confinement effect of the CO, the thickness of the palladium nanosheets is restricted to less than 10 atomic layers. The nanosheet edge length is synthetically controllable from 20 to 160 nm, leading to tunable NIR SPR. Unlike silver/gold nanostructures, the two-dimensional structure of the palladium nanosheets appears to be highly stable upon NIR irradiation. The palladium nanosheets also exhibit electrocatalytic activity for the oxidation of formic acid that is 2.5 times as active as that measured for high-surface-area (47 m^2 g^{-1}) commercial palladium black.

In a typical synthesis of palladium nanosheets, palladium(II) acetylacetonate, poly(vinylpyrrolidone) (PVP) and a halide salt were dissolved in a solvent (such as dimethylformamide (DMF), dimethylpropionamide, benzyl alcohol or benzene ethanol). The resulting homogeneous solution was transferred to a glass pressure vessel. After being charged with CO to 1 bar, the vessel was heated from room temperature to 100 °C in 30 min and kept at this temperature for 3 h with stirring. As the reaction progressed, the colour of the reaction mixture changed from yellow to light blue, and finally dark blue. The resulting blue colloidal products were collected by centrifugation, and washed several times with ethanol and acetone.

When DMF was used as the solvent, reaction in the presence of both PVP and cetyltrimethylammonium bromide (CTAB) produced colloidal palladium blue, composed of uniform hexagonal nanosheets with an edge length of 60 nm (Fig. 1a). By varying the reaction solvent and time, the edge length of the uniform nanosheets was tunable between tens and hundreds of nanometres. Regardless of their size, the nanosheets preferentially lay flat on the transmission electron microscope (TEM) grid, indicating the thin character of the nanosheets. Although normally forbidden in a face-centred cubic (fcc) structure, 1/3(422) reflections arise in the as-prepared palladium nanosheets. The fcc structure of the palladium nanosheets is supported by their X-ray diffraction (XRD) pattern (Supplementary Fig. S1). Lattice fringes with an interplanar spacing of 0.24 nm, corresponding to 1/3(422) fringes of fcc palladium, are observed in the

[1]State Key Laboratory for Physical Chemistry of Solid Surfaces and Department of Chemistry, College of Chemistry and Chemical Engineering, Xiamen University, Xiamen 361005, China, [2]Department of Physics, Xiamen University, Xiamen 361005, China. *e-mail: nfzheng@xmu.edu.cn

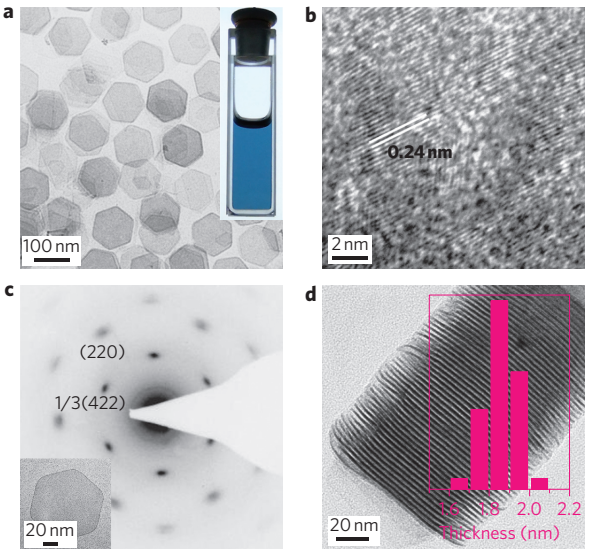

Figure 1 | Characterization of ultrathin palladium nanosheets synthesized in the presence of PVP and CTAB in DMF. a, TEM image of the palladium nanosheets. Inset: photograph of an ethanol dispersion of the as-prepared palladium nanosheets in a curvette. **b**, HRTEM image of a palladium nanosheet flat lying on the TEM grid. **c**, SAED pattern of a single palladium nanosheet (shown in the inset). **d**, TEM image of the assembly of palladium nanosheets perpendicular to the TEM grid. Inset: thickness distribution of the palladium nanosheets.

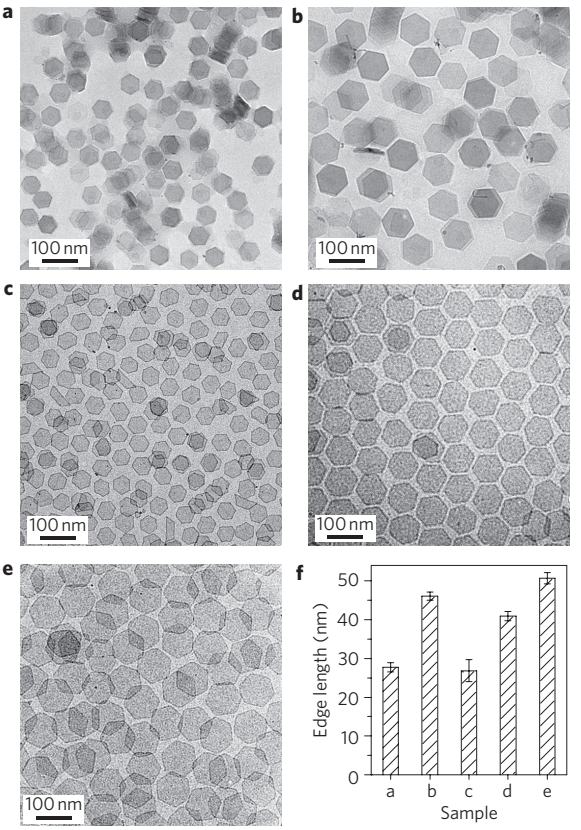

Figure 2 | TEM images of the palladium nanosheets produced under different reaction conditions. a,**b**, Palladium nanosheets, collected following 0.5 h (**a**) and 1.5 h (**b**) reactions, using CTAB as the Br^- source. **c**,**d**, Nanosheets collected following 3 h reactions using NaBr (**c**) and TBAB (**d**) as the Br^- source. **e**, Larger nanosheets, grown using the palladium nanosheets in **d** as seed particles. **f**, Edge lengths of samples **a**–**e**. Error bars in **f** are the standard deviations of the edge length distributions.

high-resolution TEM (HRTEM) image of an individual nanosheet (Fig. 1b). The appearance of 1/3(422) reflections is also confirmed by selected area electron diffraction (SAED, Fig. 1c). These results are in good agreement with previous observations on nanoplatelets of fcc metals, and suggest that the palladium nanosheets have (111) as basal planes. The appearance of stacking faults parallel to the basal (111) planes are probably associated with the palladium nanosheets[17,18,25].

The tendency of the palladium nanosheets to lie flat on the TEM grids makes it difficult to directly measure their thickness. With the presence of CTAB, we have found that the deposition of an increased concentration of palladium nanosheets on the TEM grid leads to the assembly of the nanosheets into an extended lamellar structure, which enables direct thickness measurements by TEM (Fig. 1d). Based on the analysis of more than 200 palladium nanosheets from 10 different stacks, the average thickness of the as-prepared nanosheets was found to be 1.8 nm—less than 10 atomic layers thick. The dominant exposed surfaces of the nanosheets were (111) facets. For nanosheets with an edge length of 60 nm, up to 96% of the exposed surface was (111), as verified by electrochemical CO stripping experiments in H_2SO_4. The measured CO stripping voltammetric curve (Supplementary Fig. S2) is composed of a dominant peak at 1.024 V (vs. reversible hydrogen electrode (RHE)) and a small peak (9% of total integrated charge) at 0.886 V. These two peaks correspond to the CO stripping peaks from Pd(111) and (100), respectively[26].

The use of CO is critical for growing the ultrathin palladium nanosheets. Without CO, the products contain only twinned nanoparticles (Supplementary Fig. S3). Although the importance of surfactants in producing palladium nanosheets has been suggested[27,28], we believe that the strong adsorption of CO molecules on the basal (111) planes of palladium nanosheets prevents growth along the [111] direction and is responsible for directing the formation of the sheet-like structure. The presence of CO adsorption on the (111) surfaces of the freshly prepared palladium nanosheets, before any additional CO exposure, was confirmed with CO stripping voltammetry (Supplementary Fig. S4). Fourier transform–infrared (FT-IR) studies indicate that CO was adsorbed on the surface of the palladium nanosheets predominantly in a bridge configuration. The palladium nanosheets were formed at a very early stage of the reactions. The edge length of the nanosheets increased with reaction time until the palladium precursors were depleted (Fig. 2), but their thickness remained unchanged (1.8 nm) during the reaction, as revealed by TEM measurements (Supplementary Fig. S5). This observation suggests that the six side facets of the nanosheets were the growth active sites at which the freshly reduced palladium atoms were added. The adsorption of CO molecules on the basal (111) faces of the palladium nanosheets is strong enough to confine the growth to a uniform thickness of less than 10 atomic layers. Many previous studies have demonstrated that, because of the electronic confinement effect, metallic thin films grown on semiconductor substrates can have several preferred thicknesses[2]. The reason for the preference for only one thickness in the growth of palladium nanosheets remains unclear and requires further investigation.

Although CO is key to the anisotropic growth of the palladium nanosheets, PVP serves as an effective coating to stabilize the nanosheets from agglomeration. Products obtained from reactions in the absence of PVP typically comprised aggregates of irregularly shaped palladium sheets (Supplementary Fig. S6). In addition, reactions in the presence of PVP but in the absence of CTAB yielded freestanding plate-like palladium nanostructures with inhomogeneous shapes. The results suggest that CTAB plays an important role in the preferential growth of uniform hexagonal sheets. Based

on the electrochemical CO stripping results, a small fraction of (100) planes is present in the palladium nanosheets. Considering that the basal faces of the palladium nanosheets are (111) bound by CO, the six side walls of each nanosheet probably have the lattice character of a (100) plane. The selective bonding of Br^- on (100) of fcc metals has previously been demonstrated and applied for the selective growth of palladium nanobars[29]. Therefore, we hypothesize that the Br^- in CTAB is essential for defining the hexagonal shape of the palladium nanosheets by regulating the lateral growth rate with its binding to the (100) planes. Experimentally, the presence of Br^- on the as-prepared palladium nanosheets was confirmed by both XPS and ion chromatography analysis (Supplementary Fig. S7). Consistent with the presence of Br^- on the nanosheet surface, we have measured a negative zeta potential (−25 mV) for the nanosheets. Based on the proposed growth mechanism, it should be possible to obtain hexagonal palladium nanosheets when CTAB is replaced by other Br^- salts. Indeed, well-defined hexagonal palladium nanosheets were obtained in reactions in which NaBr or NBu_4Br (TBAB) was used instead (Fig. 2), or when other halides (such as NaCl or NaI) (Supplementary Fig. S8) were applied. According to TEM measurements (Supplementary Fig. S9), all the synthesized palladium nanosheets were 1.8 nm thick.

Motivated by the fact that the optical properties of metal nanostructures are typically dependent on size, we developed three methods to control the edge length of the palladium nanosheets. First, formation kinetics studies show that the size of the nanosheets increases with reaction time. Palladium nanosheets grown in DMF for 0.5, 1.5 and 3 h had edge lengths of 28, 46 and 60 nm, respectively (Figs 1, 2a,b). Larger palladium nanosheets were also readily synthesized using smaller nanosheets as the growth seed (Fig. 2d,e). Furthermore, the edge length of the palladium nanosheets was controllable by varying the reaction solvent. The average edge lengths for nanosheets produced in 3 h reactions using dimethylpropionamide, 2-phenylethanol and benzyl alcohol as the solvent were 35, 125 and 160 nm, respectively (Supplementary Fig. S10).

The most striking feature of our utrathin hexagonal palladium nanosheets is that they exhibit well-defined size-dependent and therefore tunable absorption peaks in the NIR region (Fig. 3a). Palladium nanosheets dispersed in ethanol and kept at 0 °C for two months retained their NIR absorption, but no CO could be detected adsorbed on the palladium by CO oxidative stripping measurements (Supplementary Fig. S11). We therefore excluded the possibility that the absorption of the palladium nanosheets arises from the charge transfer between palladium and CO. The SPR peak of the palladium nanosheets redshifted from 826 to 992, 1,045 and 1,068 nm when the edge length was increased from 21 to 27, 41 and 51 nm, respectively (Fig. 3a, Supplementary Fig. S10). As confirmed by TEM analysis, all the examined nanosheets had a fixed thickness of 1.8 nm (Supplementary Fig. S9). The ultrathin nature of the palladium nanosheets is key to their unique SPR in the NIR region. As suggested by the calculations of extinction spectra using the discrete dipole approximation (DDA) method (Supplementary Fig. S12), the aspect ratio R, where R is the edge length divided by the thickness of the hexagonal nanosheets, plays an essential role in determining the SPR properties of the palladium nanosheets. When the edge length was fixed at 21 nm, the extinction peaks of the hexagonal palladium nanosheets were calculated at 467, 578, 684 and 860 nm for thicknesses of 6, 4, 3 and 2 nm, respectively. For palladium nanosheets with fixed thickness at 2 nm, the calculations also showed that a longer edge and thus a larger R led to the redshift of the SPR peak of the nanosheets, consistent with our experimental observations. More importantly, the nanosheets have high extinction coefficients in the NIR region. The extinction coefficient for the nanosheets with an edge size of 41 nm was measured as 4.1×10^9 $M^{-1}\,cm^{-1}$ at 1,045 nm

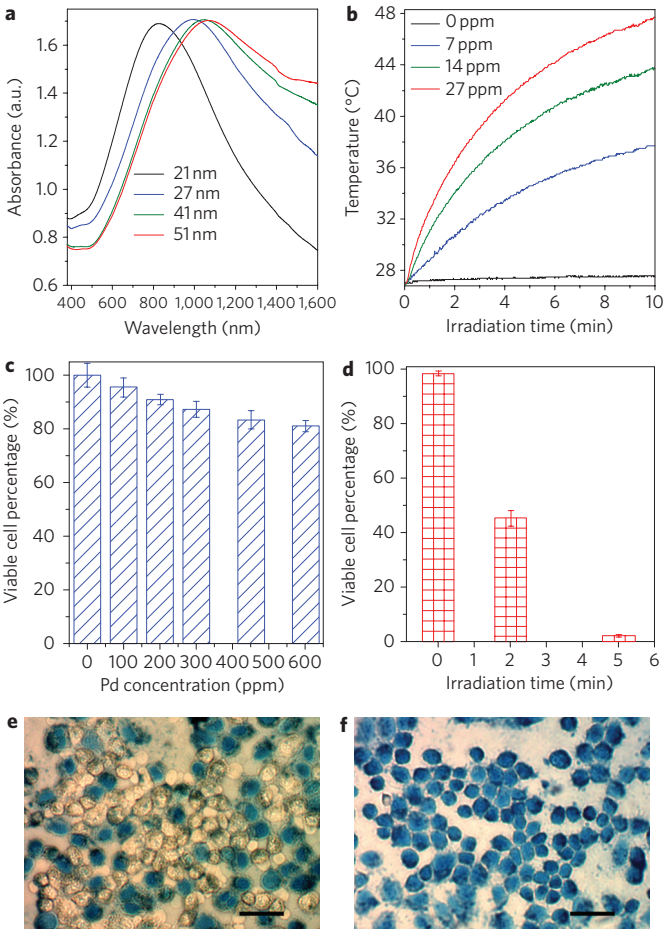

Figure 3 | Optical absorption and photothermal properties of palladium nanosheets. a, Absorption spectra of hexagonal palladium nanosheets with average edge lengths of 21, 27, 41 and 51 nm. **b**, Photothermal effect of palladium nanosheets. The temperature versus time plots were recorded for various concentrations of palladium nanosheets (edge length, 41 nm) on irradiation by a 1 W laser. **c**, Viability of healthy liver cells incubated for 48 h with different concentrations of palladium nanosheets. **d**, Viability of human hepatoma cells upon irradiation by an 808 nm laser with a power density of 1.4 W cm^{-2} for various periods. Before irradiation, the cells were incubated with palladium nanosheets (20 μg ml^{-1}) for 12 h. Cell viabilities were measured by standard MTT assay. **e**,**f**, Micrographs corresponding to 2 min (**e**) and 5 min (**f**) irradiation. Dead cells are stained with trypan blue. Error bars in **c** and **d** are the standard deviations of the means of five independent determinations. Scale bars, 50 μm.

(Supplementary Fig. S13). This number is comparable to those reported for gold nanorods[30]. Owing to their strong NIR absorption features, these palladium nanosheets are of interest for use in photothermal tumour therapy.

The photothermal effect induced by NIR SPR absorption was investigated by monitoring the temperature of 1 ml aqueous solutions of various concentration of palladium (0, 7, 14 and 27 ppm) irradiated by a NIR laser (808 nm, 1 W). As shown in Fig. 3b, the temperature of the solution containing 27 ppm palladium rose from 28.0 to 48.7 °C after 10 min of irradiation. In comparison, the temperature of the solution in the absence of palladium nanosheets increased by only 0.5 °C. Compared to silver and gold nanostructures with a NIR photothermal effect, the palladium nanosheets also exhibit improved photothermal stability. Upon irradiation for 30 min with a 2 W, 808 nm laser, the sheet-like structure of the palladium nanosheets was retained well (Supplementary

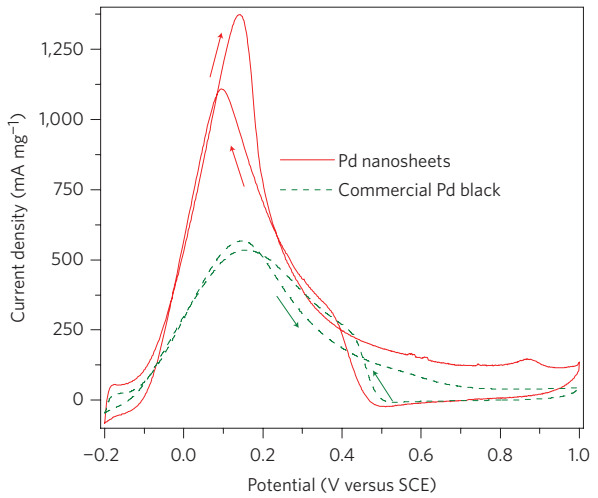

Figure 4 | Comparison of electrocatalytic properties of palladium nanosheets and palladium black. The CV curves were recorded in an aqueous solution containing 0.5 M H_2SO_4 and 0.25 M HCOOH at a scan rate of 50 mV s^{-1}. Edge size of palladium nanosheets, 41 nm; palladium black from Aldrich (47 m^2 g^{-1}).

Fig. S14), leading to a good SPR response in the NIR region (Supplementary Fig. S15), whereas silver and gold nanoprisms were severely distorted under a similar irradiation power (Supplementary Fig. S16). Furthermore, the as-prepared palladium nanosheets appear to be largely biocompatible; the viable cell count for healthy liver cells was reduced by only 20% after 48 h of exposure to a 600 μg ml^{-1} solution of palladium nanosheets (Fig. 3c). By incubating liver cancer cells with polyethyleneimine-exchanged palladium nanosheets, ~100% of the cells were killed after 5 min of irradiation with an 808 nm laser providing 1.4 W cm^{-2} (Fig. 3d–f). The photothermal cell-killing efficacy was also confirmed by 3-(4,5-dimethylthiazol-2-yl)-2,5-diphenyltetrazolium bromide (MTT) assay and is comparable or higher than that reported for gold nanostructures[31–33].

Furthermore, owing to their ultrathin character, the palladium nanosheets have a high surface area. To measure the electrochemically active surface area of the nanosheets, cyclic voltammograms (CV) were recorded in a solution of sulphuric acid. Given the known charge associated with the electrochemical absorption/desorption of a monolayer of hydrogen on the (111) face of palladium (210 μC cm^{-2}), the electrochemically active surface area of the nanosheets was calculated to be as high as 67 m^2 g^{-1} for the palladium nanosheets with an edge length of 41 nm (Supplementary Fig. S17). This is slightly lower than the theoretical maximum surface area (~100 m^2 g^{-1}) calculated from the measured nanosheet geometry. The nanosheets had excellent electrocatalytic activity for the oxidation of formic acid (Fig. 4). The maximum current densities of the deposited nanosheets were measured to be 1,380 mA mg^{-1} at 0.14 V (vs. saturated calomel electrode (SCE)), 2.5 times as active as that obtained using a commercial palladium black (47 m^2 g^{-1} from Aldrich, Supplementary Fig. S18).

In conclusion, we have demonstrated the facile synthesis of hexagonal palladium nanosheets that are less than 10 atomic layers thick, and have controllable edge length and tunable NIR SPR features. Upon NIR irradiation, the as-prepared colloidal palladium blue creates a significant photothermal effect and effectively kills cancer cells. In comparison with other noble metal nanostructures composed of silver and/or gold, a key advantage of these palladium nanosheets is that they do not undergo a shape transformation into spherical particles upon irradiation with a high-power NIR laser. In addition, the palladium nanosheets exhibit high electrocatalytic activity for formic acid oxidation.

Received 14 July 2010; accepted 29 October 2010; published online 5 December 2010

References

1. Smith, A. R., Chao, K. J., Niu, Q. & Shih, C. K. Formation of atomically flat silver films on GaAs with a 'silver mean' quasi periodicity. *Science* **273,** 226–228 (1996).
2. Zhang, Z. Y., Niu, Q. & Shih, C. K. 'Electronic growth' of metallic overlayers on semiconductor substrates. *Phys. Rev. Lett.* **80,** 5381–5384 (1998).
3. Paggel, J. J., Miller, T. & Chiang, T. C. Quantum-well states as Fabry–Perot modes in a thin-film electron interferometer. *Science* **283,** 1709–1711 (1999).
4. Guo, Y. *et al.* Superconductivity modulated by quantum size effects. *Science* **306,** 1915–1917 (2004).
5. Qin, S. Y., Kim, J., Niu, Q. & Shih, C. K. Superconductivity at the two-dimensional limit. *Science* **324,** 1314–1317 (2009).
6. Ozer, M. M. *et al.* Tuning the quantum stability and superconductivity of ultrathin metal alloys. *Science* **316,** 1594–1597 (2007).
7. Campbell, C. T. Ultrathin metal films and particles on oxide surfaces: structural, electronic and chemisorptive properties. *Surf. Sci. Rep.* **27,** 1–111 (1997).
8. Gordon, R., Sinton, D., Kavanagh, K. L. & Brolo, A. G. A new generation of sensors based on extraordinary optical transmission. *Acc. Chem. Res.* **41,** 1049–1057 (2008).
9. Langhammer, C., Yuan, Z., Zoric, I. & Kasemo, B. Plasmonic properties of supported Pt and Pd nanostructures. *Nano Lett.* **6,** 833–838 (2006).
10. Lal, S., Clare, S. E. & Halas, N. J. Nanoshell-enabled photothermal cancer therapy: impending clinical impact. *Acc. Chem. Res.* **41,** 1842–1851 (2008).
11. Jain, P. K., Huang, X. H., El-Sayed, I. H. & El-Sayed, M. A. Noble metals on the nanoscale: optical and photothermal properties and some applications in imaging, sensing, biology, and medicine. *Acc. Chem. Res.* **41,** 1578–1586 (2008).
12. Skrabalak, S. E. *et al.* Gold nanocages: synthesis, properties, and applications. *Acc. Chem. Res.* **41,** 1587–1595 (2008).
13. Calander, N. Molecular detection and analysis by using surface plasmon resonances. *Curr. Anal. Chem.* **2,** 203–211 (2006).
14. Schaadt, D. M., Feng, B. & Yu, E. T. Enhanced semiconductor optical absorption via surface plasmon excitation in metal nanoparticles. *Appl. Phys. Lett.* **86,** 063106 (2005).
15. Krenn, J. R. Nanoparticle waveguides—watching energy transfer. *Nature Mater.* **2,** 210–211 (2003).
16. Larsson, E. M., Langhammer, C., Zoric, I. & Kasemo, B. Nanoplasmonic probes of catalytic reactions. *Science* **326,** 1091–1094 (2009).
17. Jin, R. C. *et al.* Controlling anisotropic nanoparticle growth through plasmon excitation. *Nature* **425,** 487–490 (2003).
18. Jin, R. C. *et al.* Photoinduced conversion of silver nanospheres to nanoprisms. *Science* **294,** 1901–1903 (2001).
19. Murphy, C. J. *et al.* Anisotropic metal nanoparticles: synthesis, assembly, and optical applications. *J. Phys. Chem. B* **109,** 13857–13870 (2005).
20. Jain, P. K., Huang, X. H., El-Sayed, I. H. & El-Sayad, M. A. Review of some interesting surface plasmon resonance-enhanced properties of noble metal nanoparticles and their applications to biosystems. *Plasmonics* **2,** 107–118 (2007).
21. Link, S. *et al.* Laser photothermal melting and fragmentation of gold nanorods: energy and laser pulse-width dependence. *J. Phys. Chem. A* **103,** 1165–1170 (1999).
22. Yavuz, M. S. *et al.* Gold nanocages covered by smart polymers for controlled release with near-infrared light. *Nature Mater.* **8,** 935–939 (2009).
23. Xia, Y., Xiong, Y. J., Lim, B. & Skrabalak, S. E. Shape-controlled synthesis of metal nanocrystals: simple chemistry meets complex physics? *Angew. Chem. Int. Ed.* **48,** 60–103 (2009).
24. Xiong, Y. J. & Xia, Y. N. Shape-controlled synthesis of metal nanostructures: the case of palladium. *Adv. Mater.* **19,** 3385–3391 (2007).
25. Germain, V. *et al.* Stacking faults in formation of silver nanodisks. *J. Phys. Chem. B* **107,** 8717–8720 (2003).
26. Hara, M., Linke, U. & Wandlowski, T. Preparation and electrochemical characterization of palladium single crystal electrodes in 0.1 M H_2SO_4 and $HClO_4$ part I. Low-index phases. *Electrochim. Acta* **52,** 5733–5748 (2007).
27. Schlotterbeck, U. *et al.* Shape-selective synthesis of palladium nanoparticles stabilized by highly branched amphiphilic polymers. *Adv. Funct. Mater.* **14,** 999–1004 (2004).
28. Siril, P. F. *et al.* Synthesis of ultrathin hexagonal palladium nanosheets. *Chem. Mater.* **21,** 5170–5174 (2009).
29. Xiong, Y. J. *et al.* Synthesis and mechanistic study of palladium nanobars and nanorods. *J. Am. Chem. Soc.* **129,** 3665–3675 (2007).

30. Orendorff, C. J. & Murphy, C. J. Quantitation of metal content in the silver-assisted growth of gold nanorods. *J. Phys. Chem. B* **110,** 3990–3994 (2006).
31. Huang, X. H., El-Sayed, I. H., Qian, W. & El-Sayed, M. A. Cancer cell imaging and photothermal therapy in the near-infrared region by using gold nanorods. *J. Am. Chem. Soc.* **128,** 2115–2120 (2006).
32. Hirsch, L. R. *et al.* Nanoshell-mediated near-infrared thermal therapy of tumors under magnetic resonance guidance. *Proc. Natl Acad. Sci. USA* **100,** 13549–13554 (2003).
33. Chen, J. Y. *et al.* Immuno gold nanocages with tailored optical properties for targeted photothermal destruction of cancer cells. *Nano Lett.* **7,** 1318–1322 (2007).

Acknowledgements

The authors acknowledge helpful discussions with L.S. Zheng, Z.Q. Tian, G.D. Stucky, Z.X. Xie and B.W. Mao. The authors also thank S.W. Boettcher and Z.P. Zheng for suggestions and editing of the English. This work was supported by the NSF of China (20925103, 20871100, 20721001 and 20703032), MOST of China (2009CB930703, 2011CB932403), the Fok Ying Tung Education Foundation (121011), NSF of Fujian for a Distinguished Young Investigator Grant (2009J06005) and the Key Scientific Project of Fujian Province (2009HZ0002-1).

Author contributions

X.Q.H. performed the experiments, collected and analysed the data, and wrote the paper. S.H.T. carried out the apoptosis assay and *in vitro* photothermal therapy tests. X.L.M. was responsible for AFM analysis. Y.D. and G.X.C. helped with synthesis of the materials. Z.Y.Z. helped with the electrochemical and FTIR measurements. F.X.R. and Z.L.Y. carried out the calculations of extinction spectra. N.F.Z. conceived the experiments, planned the synthesis, analysed the results and wrote the paper.

Additional information

The authors declare no competing financial interests. Supplementary information accompanies this paper at www.nature.com/naturenanotechnology. Reprints and permission information is available online at http://npg.nature.com/reprintsandpermissions/. Correspondence and requests for materials should be addressed to N.F.Z.